Visibility of coronal mass ejections as a function of flare location and intensity

S. Yashiro,[1,2] N. Gopalswamy,[3] S. Akiyama,[1,2] G. Michalek,[1,2,4] and R. A. Howard[5]

[1] We report the visibility (detection efficiency) of coronal mass ejections (CMEs) of the Large Angle Spectrometric Coronagraph (LASCO) on board the Solar and Heliospheric Observatory (SOHO). We collected 1301 X-ray flare events (above C3 level) detected by the GOES satellite and examined their CME associations using data from LASCO coronagraphs. The CME visibility was examined using the longitudinal variation of CME association of X-ray flares, under the assumption that all CMEs associated with limb flares are detectable by LASCO. Our findings are (1) the CME association rate clearly increased with X-ray flare size from 20% for C-class flares (between C3 and C9 levels) to 100% for huge flares (above X3 level), (2) all CMEs associated with X-class flares were detected by the LASCO coronagraphs, while half (25–67%) of CMEs associated with C-class flares were invisible. We examined the statistical properties of the flare-associated CMEs and compared them by flare size and longitude. CMEs associated with X-class flares were significantly faster (median 1556 km/s) and wider (median 244°) than those of CMEs associated with disk C-class flares (432 km/s, 68°). We conclude that all fast and wide CMEs are detectable by LASCO, but slow and narrow CMEs may not be visible when the CMEs originate from the disk center.

Citation: Yashiro, S., N. Gopalswamy, S. Akiyama, G. Michalek, and R. A. Howard (2005), Visibility of coronal mass ejections as a function of flare location and intensity, *J. Geophys. Res.*, *110*, A12S05, doi:10.1029/2005JA011151.

1. Introduction

[2] Coronal mass ejections (CMEs) from the Sun are among the main heliospheric disturbances. The Earth-directed CMEs are important for space weather research since they can produce severe geomagnetic storms. Usually, the Earth-directed CMEs are seen as halo CMEs, whose material entirely surrounds the coronagraph occulting disk [*Howard et al.*, 1982]. However, the Earth-directed CMEs are the most difficult CMEs to observe due to the nature of coronagraphic observations. Since coronagraphs detect the Thomson-scattered photospheric light, the CME brightness depends on (electron) column density, height (=distance from the photosphere), and scattering angle. The first two factors are dominant; thus the CME is brighter when the CME is closer to the Sun (the CME density decreases with height, since the CME expands in both radial and transverse directions). Therefore the detection efficiency of the Earth-directed CMEs is lower, since the CMEs are farther from the Sun when the CME material reaches above the coronagraph occulting disk (see Appendix A of *Hundhausen*

[1993], *Vourlidas et al.* [2000], and *Andrews* [2002] for details).

[3] Even if coronagraphs properly observe the solar corona with good cadence, extremely faint CMEs cannot be observed. We call such CMEs invisible CMEs. The visibility function (V) is the probability of CME identification defined as $V = N_{obs}/N_{total}$, where N_{obs} is the number of observed CMEs and N_{total} is the total number of CMEs. Since there is no method to find N_{total}, we need assumptions to determine the visibility function. It was assumed that all metric type II bursts have associated CMEs, and the lack of CMEs with metric type II was considered to be due to invisible CMEs. In this case, the visibility function is determined as $V = N_{obs}/N_{TypeII}$, where N_{TypeII} is the number of type II radio bursts. Results published using data from the Solar Maximum Mission (SMM) and Solwind coronagraphs found significant longitudinal variations in the CME associations of flares [*Kahler et al.*, 1984; *Sawyer*, 1985; *Webb and Howard*, 1994; *Burkepile et al.*, 1994]. Since the inherent CME associations must be constant for any longitude, the difference of CME associations between disk and limb flares can be considered due to longitudinal variation of visibility function. Under the assumption that all CMEs associated with limb flares can be observed, the visibility function of CMEs associated with disk flares (V_{disk}) is determined as $V_{disk} = R_{disk}/R_{limb}$, where R_{disk} and R_{limb} are the CME association rate of disk and limb flares, respectively.

[4] The Large Angle and Spectrometric Coronagraphs (LASCO) [*Brueckner et al.*, 1995] on the Solar and Heliospheric Observatory (SOHO) [*Domingo et al.*, 1995] space-

---

[1]Catholic University of America, Washington, D.C., USA.
[2]Also at NASA Goddard Space Flight Center, Greenbelt, Maryland, USA.
[3]NASA Goddard Space Flight Center, Greenbelt, Maryland, USA.
[4]Also at Astronomical Observatory of Jagiellonian University, Krakow, Poland.
[5]Naval Research Laboratory, Washington, D.C., USA.

craft have observed more than 9000 CMEs from 1996 through 2004. The superior capabilities of the LASCO coronagraphs enable us to detect a larger number of faint CMEs than was possible by previous coronagraphs [*Howard et al.*, 1997; *St. Cyr et al.*, 2000]. Under the assumption of all metric type II bursts having associated CMEs, *St. Cyr et al.* [2000] carried out a preliminary analysis of the visibility function of LASCO CMEs. They found that 95% (76/80) of metric Type II bursts were associated with LASCO CMEs and concluded that the LASCO coronagraphs observe almost all CMEs. *Andrews* [2003] examined CME association of 311 large X-ray flares (above M-class) and reported that there was no significant longitudinal variation in the CME association, suggesting that all CMEs associated with large flares are detectable by LASCO. In the meanwhile, *Gopalswamy et al.* [2001] reported that 11 out of 34 metric type II bursts from source longitudes <60° were not associated with LASCO CMEs, indicating approximately a third of CMEs originating from the disk center were invisible to LASCO. In addition, from the longitudinal variation of CME association with EIT waves [*Biesecker et al.*, 2002], *Cliver et al.* [2005] estimated 40% of the CMEs from source longitudes <60° are invisible to LASCO. Different visibilities have been reported in various studies, since the visibility would be different between energetic and average CMEs.

[5] The relation between CMEs and other phenomena has been extensively investigated by many researchers (*Munro et al.* [1979]; see *Kahler* [1992] for reviews), and it has been established that the CMEs associated with large X-ray flares are likely to be fast and wide [*Gosling et al.*, 1976; *MacQueen and Fisher*, 1983; *Kahler et al.*, 1989; *Burkepile et al.*, 1994, 2004; *Moon et al.*, 2002]. Thus it is possible to determine the visibility functions of both energetic and average CMEs from the CME association of large and average X-ray flares, respectively. In this paper, we examined CME association as a function of flare longitude not only for large flares but also for average flares. Then, the visibility functions of CMEs were determined from the longitudinal variation of the CME association rate, with the assumption that all limb CMEs are detectable by LASCO. (The disk and limb events are defined as those with flare longitude in the range 0°–29° and 60°–90°, respectively. CMEs associated with the disk (limb) flares are called disk (limb) CMEs. Events occurring between these longitudes are called intermediate events). We also examined the basic properties (projected speed, angular width, and final measurement height) of flare-associated CMEs to gain insight into the flare-CME relationship as a function of flare location.

2. X-Ray Flare and CME Data

[6] NOAA GOES satellites monitor X-ray flux from the Sun in two bands covering 1.0–8.0Å and 0.5–4.0Å and routinely identify X-ray flares. The size of an X-ray flare is labeled by the peak X-ray flux in the lower-energy band (1.0–8.0Å). Flare peak flux is denoted by Cn, Mn, Xn, where C, M, and X denote the X-ray flux levels of 10^{-6}, 10^{-5}, and 10^{-4} [Wm^{-2}] respectively, and n is a coefficient to indicate the actual flux. For example, a M5 flare would have a peak flux of 5×10^{-5} [W m^{-2}]. We

compiled X-ray flares above the C3 level from the online solar event lists reported by the NOAA Space Environment Center (http://www.sec.noaa.gov/ftpmenu/indices.html). We did not include flares below C3 level because it is hard to identify the associated CMEs for small flares. We choose C3 level as a criterion, since C3 level ($10^{-5.52}$ [W m^{-2}]) is the middle value of C1 (10^{-6} [W m^{-2}]) and M1 (10^{-5} [W m^{-2}]) on a logarithmic scale. When we say C-class flares in this paper, we mean flares with peak intensity C3 and above. There were 60 X-class, 814 M-class, and 2956 C-class flares from 1996 through 2001.

[7] In obtaining the CME association rate as a function of flare longitude, the location of the X-ray source is quite important. The NOAA solar event lists contain the location of the associated Hα flare for many X-ray flares. When the locations of M- and X-class flares were not listed, we identified their location using SOHO's Extreme ultraviolet Imaging Telescope (EIT) and Yohkoh's Soft X-ray Telescope (SXT) data. It is not hard to determine the location for large flares from EUV observations but not easy for C-class flares. X-ray images are the best to determine the location of X-ray flares, so we required the C-class flares to have both Hα flare location and SXT observations. Of the 2956 C-class flares, only 852 passed this criterion, but the number was reasonable enough to examine their CME associations. Note this criterion was applied to C-class flares only. We also excluded events for which two or more flares occurred in different active regions at the same time.

[8] All white light data of coronal mass ejections in this study were obtained by LASCO. Near-Sun observations are necessary for accurate identification of CMEs associated with X-ray flares. The innermost C1 telescope was the best, but it operated only for the first 2.5 years of the mission. We required at least two white light images from the C2 coronagraph to be available for the period 0–2 hours after the X-ray flare onset. This criterion excluded the events during occasional LASCO data gaps, including a huge data gap from June to October 1998. Even if LASCO operated normally, we could not examine whether or not a flare was associated with a CME when the LASCO images were contaminated by solar energetic particles ("snow storm"). Additionally, when a large prominent CME was progressing, we could not identify small CMEs in the aftermath. Therefore we did not include these events in our analysis. Applying all of the selection criteria described above left 49 X-class, 610 M-class, and 642 C-class flares with comprehensive white light observations.

3. CME Associations

[9] We used the SOHO/LASCO CME Catalog (http://cdaw.gsfc.nasa.gov/) [*Yashiro et al.*, 2004] to investigate the CME associations. Almost all CMEs detected by the LASCO C2 and C3 coronagraphs and their basic properties have been compiled in this catalog. The onset times of all LASCO CMEs are recorded in the height-time text files in the catalog. The onset time of each CME is estimated by a first- or second-order extrapolation (constant speed and constant acceleration, respectively) of the CME trajectory to the solar limb. Since we assume that all CMEs are limb events, the error in the obtained CME onset is large for disk events. Thus we used these onsets only for finding prelim-

Table 1. CME Association Rate and Number of Flares With/Without CMEs

| Class		Disk Events	Intermediate	Limb Events	All
X	Rate	91%	100%	82% (79−86%)	91% (90−92%)
	Certain	20	13	11	44
	Uncertain	0	0	1	1
	No CME	2	0	2	4
	Subtotal	22	13	14	49
M	Rate	43% (36−51%)	51% (44−58%)	51% (46−57%)	49% (42−55%)
	Certain	65	79	115	259
	Uncertain	26	26	27	79
	No CME	89	75	108	272
	Subtotal	180	180	250	610
C	Rate	15% (12−18%)	20% (16−25%)	30% (24−36%)	20% (16−25%)
	Certain	32	33	39	104
	Uncertain	15	20	19	54
	No CME	221	159	104	484
	Subtotal	268	212	162	642

inary CME candidates. We applied a 3-hour time window (90 min before and 90 min after the onset of X-ray flares) to find the candidates. When an X-ray flare did not have any CME candidates in the 3-hour time window, we checked the original LASCO images to find any missing CMEs.

[10] We then checked the consistency of the association between X-ray flares and CME candidates, since the time window analysis by itself could produce false flare-CME associations. For example, there is only a small difference in the CME visibility between frontside and backside events [see *Andrews*, 2002], so it is next to impossible to distinguish them only by coronagraph observations. Therefore the time window analysis would determine a frontside flare and a backside CME as an associated pair. In order to avoid the false flare-CME associations, we checked lower corona images obtained by EIT and SXT to confirm that the CME originates from the frontside. The check points used were (1) CME and flare locations, (2) eruptive surface activity (e.g., filament eruption, dimming), and (3) timing of CME and flare onsets. Except for disk events, the associated CMEs must appear above the flares [*Harrison*, 1986]. If the associated CME appeared from the opposite hemisphere, we treated it as a false association. The CME onsets were estimated again by a first- or second-order extrapolation to the flare location (not solar limb), and the onset time difference (T_d) was used as a guide, since not all eruptive flares have prominent eruptive signature in EIT or SXT images. A CME-flare pair with $T_d < 30$ min was considered a certain (true) association unless EIT or SXT images showed any surface signatures indicating the CME originating from a different source region. Conversely, even for $T_d > 30$ min, if EIT or SXT images showed an eruptive signature connecting the flare and CME, we treated it as a certain (true) association. However, we cannot decide the associations mechanically, since the identification of eruptive signature is subjective. When it was hard to give a clear-cut true or false answer for a flare-CME pair, we treated it as an uncertain association.

[11] Table 1 summarizes the results of CME associations of X-ray flares by longitude of flare location and flare class. We examined the CME association of 1301 X-ray flares and found 407 to be certainly associated with CMEs (indicated as "certain"). The majority were flares without associated CMEs (760 flares; indicated as "no CME"). We could not determine whether or not the remaining 134 flares were associated with CMEs (indicated as "uncertain"). The numbers of flares in each category by flare intensity and location are shown in Table 1. We assumed that half of the uncertain events had true association and then determined the CME association rate by dividing the number of flares with CMEs by total number of flares. The lower errors are the fractions of flares certainly associated with CMEs (equivalent to assuming all of the uncertain event had no associated CME), and the upper errors are obtained by dividing the number of flares with both certain and uncertain CMEs by total number of flares (equivalent to assuming all of the uncertain event had associated CME).

[12] In order to determine the CME association rate as a function of the peak X-ray intensity, the data are divided into five bins: C3.0−C9.9, M1.0−M2.9, M3.0−M9.9, X1.0−X2.9, and X3.0 and above. Except for the last bin, the bin size is nearly constant on a logarithmic scale. Figure 1 shows the CME association rates as a function of the peak X-ray intensity for disk (light) and limb events (dark). There is no error bar for the last bin, since there is no uncertain association for flares greater than the X3 level. It is clear that the CME association rate of X-ray flares increases with peak X-ray intensity, the same as in previous results [e.g., *Kahler et al.*, 1989]. Only 15% of disk C-class flares had associated CMEs. The limb flares had more CMEs (30%) since CMEs are most visible when they originate from the limb. The CME association rates for M-class flares are 43% for disk events and 51% for limb events. This association rate is similar to that of *Andrews* [2003], who reported 55% for M-class flares. The CME association rates for the flares between X1 and X3 levels are 91% for disk events and 82% for limb events. All of the eight huge flares (above X3 level) in our data set had associated CMEs. However, we cannot claim that >X3 flares are indicative of CME association, since our data sample is too small. In addition, *Feynman and Hundhausen*
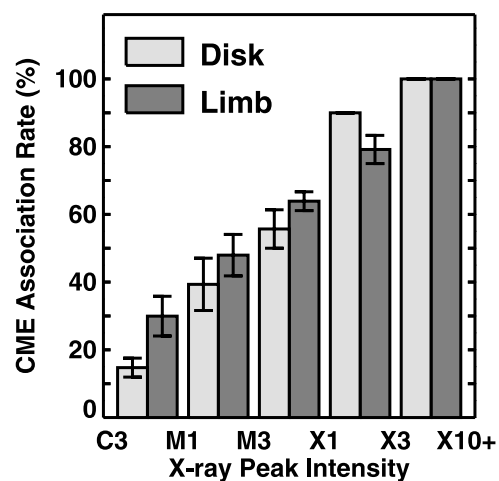
Figure 1. Coronal mass ejection (CME) association rate of disk (light) and limb (dark) flares as a function of X-ray flare size. The last bin includes >X10 flares.

Table 2. X-Class Flares Without Associated CMEs

Date	Start	Peak	End	Class	Location	NOAA	Type II
2000/06/06	1330	1339	1346	X1.1	N20E18	9026	N
2000/09/30[a]	2313	2321	2328	X1.2	N07W91	9169	N
2001/04/02	1004	1014	1020	X1.4	N17W60	9393	N
2001/06/23	0402	0408	0411	X1.2	N10W23	9511	N

[a]The X1.2 flare on 2000 September 30 was reported by *Green et al.* [2002].

[1994] reported that an X4 flare on 9 March 1989 had no associated CME from SMM observations.

3.1. X-Class Flares Without Associated CMEs

[13] Many X-class flares are associated with CMEs, but some are certainly without CMEs. There are only few reports of X-class flares without associated CMEs [*Feynman and Hundhausen*, 1994; *Green et al.*, 2002]. They found that the X-class flares without associated CMEs were compact (or confined) and short-lived.

[14] Four X-class flares in our list had no CMEs (see Table 2). We carefully reexamined these four events, but we could not find possible CME candidates. Even though two out of the four were limb events, no associated CMEs were observed. There was no data gap and the LASCO images were not contaminated by energetic particles. We have no doubt they had no CMEs except for one event. The X1.1 flare on 6 June 2000 at 1330 UT was a difficult event to find whether the flare had an associated CME or not. This is because there was an M7.1 flare at 1356 UT, which was associated with a CME at 1454 UT. It is possible that the X-class flare was associated with a small slow CME with speed <150 km/s, which was overtaken by the next CME at 1454 UT. However, as we describe later in section 4.1, the CMEs associated with X-class flares are very fast, thus we consider this flare to have had no CME.

[15] Table 2 summarizes the four X-class flares without associated CMEs. In columns 2, 3, and 4, we have listed the start, peak, and end time of X-ray flares, respectively. In columns 5, 6, and 7, we have listed X-ray class, heliographic location, and NOAA active region number. The duration of X-class flares without associated CMEs ranges from 9 to 16 min, which is much shorter than the average duration (36 min) of X-class flares with associated CMEs. Therefore as reported previously, all X-class flares without associated CMEs were short-lived (impulsive). Whether or not an X-class flare was associated with metric type II radio burst is noted in column 8. All four events were not associated with metric type IIs. This result is consistent with the four X-class flares not having associated CMEs.

3.2. Visibility Function of LASCO CMEs

[16] Figure 2 shows the CME association rates of X-class (top), M-class (middle), and C-class (bottom) flares as functions of the flare longitude. The error bars are determined by the same method as in Figure 1. For the X-class flares, as we noted previously, even limb X-class flares can lack an associated CME. There was no tendency for the CME association rate of disk flares to be lower than that of limb flares; thus the lack of association was not likely due to a problem with the visibility resulting from the Thomson scattering. Therefore we conclude that all CMEs associated with X-class flares were visible if they existed.

[17] For the M-class flares, the CME association rates were almost flat (~51%) for limb and intermediate longitude but slightly low (~43%) for disk events (see Figure 2b). The ratio of these two association rates indicates that ~16% of disk CMEs associated with M-class flares were invisible to LASCO coronagraphs. However, the error ranges of the CME association rates were 36–51% for disk events and
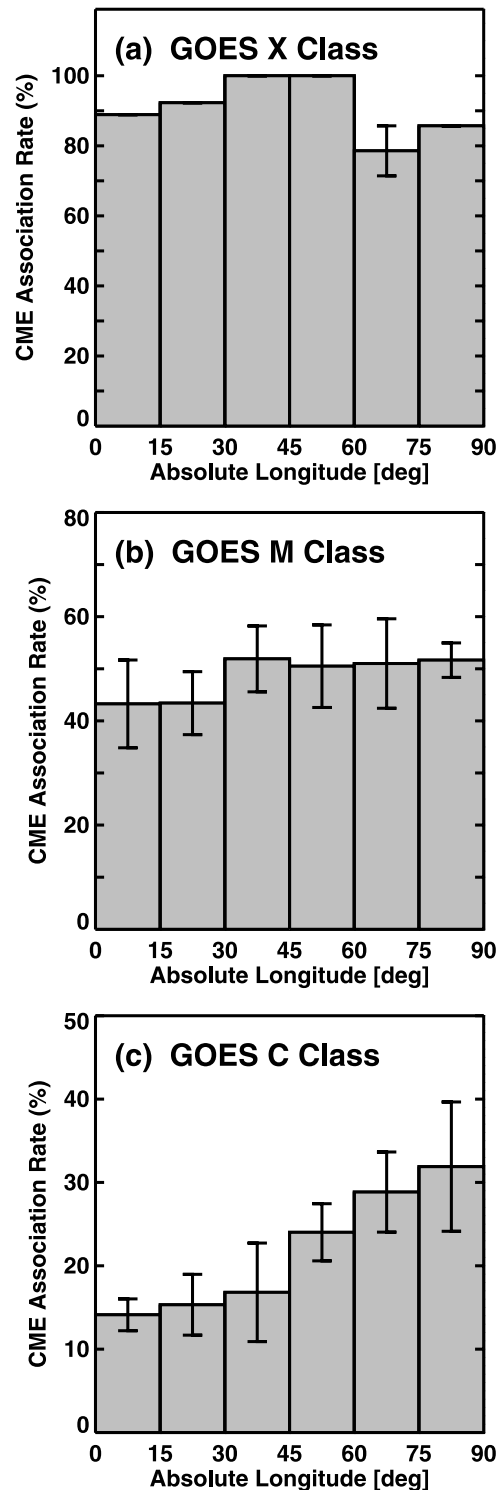
Figure 2. CME association rate as a function of longitude of X-ray flare location.

46–57% for limb events, respectively. The error range allows a flat association rate between disk and limb events, indicating no invisible CMEs. Additionally, though we assume that half of the uncertain events are true associations, the difficulty in identifying the flare-CME pair could be different: limb events are easier to identify than the disk events, suggesting that the uncertain pairs of disk events might include more true associations. Therefore the percentage of invisible disk CMEs is thought to be smaller than 16%.

[18] We found a significant difference between the limb and disk events in the CME association rates of C-class flares. Figure 2c shows the clear trend that CME association rates of limb flares are higher than those of disk flares. The CME association rates are 15% (12–18%) and 30% (24–36%) for the disk and limb events, respectively. The ratio indicates that 50% of disk CMEs were invisible with the assumption that all limb CMEs are visible. From the minimum and maximum association rates of limb and disk events, the extreme range of invisible disk CMEs was 25–67%. However, the assumption that all limb CMEs associated with C-class flares are visible may not be reasonable, since those CMEs are slow, narrow, and faint as described in the next section. If this is the case, the percentage of invisible disk CMEs is more than 50%. Conversely, it is possible that we overestimated the CME association rate of limb flares due to backside events. (It is next to impossible to distinguish whether a CME originated from W90 or from W120 region.) If this is the case, the percentage of invisible disk CMEs is less than 50%.

4. Properties of Flare-Associated CMEs

[19] As described in section 3, we found that all CMEs associated with X-class flares are detectable by LASCO coronagraphs, while about half of the CMEs associated with C-class flares are invisible. This result indicates that the CMEs associated with larger flares are brighter. It is known that the CMEs associated with large X-ray flares are likely to be fast and wide. Therefore one might think that the CMEs associated with small disk flares are likely to be invisible, since these CMEs are likely to be slow and narrow. In order to check this, we compared the basic CME properties for the different classes of flare sizes.

[20] The projection effects are also an important issue in the CME observations. Since coronagraphs observe the white light images projected onto the sky plane, a CME is observed broadside when the associated flare is located near the limb. Its apparent distance from the limb can be considered as the height of the CME apex, so the real ejection speed of the CME can be measured. On the other hand, the CME is observed in top view when the associated flare is located at the disk center and the CME propagates toward the Earth. The apparent motion of the halo CME indicates the speed of the CME flank (expansion speed). Because we are interested in the ejection (radial) speed rather than the expansion (transverse) speed, the projection effects are minimized when the CMEs occur near the sky plane.

[21] The projection effects of basic CME properties have been examined and discussed in many studies [e.g., *Hundhausen et al.*, 1994; *Gopalswamy et al.*, 2000;

Burkepile et al., 2004] and correction methods have been developed (Appendix A of *Leblanc et al.* [2001] and *Michalek et al.* [2003]). One of the basic models to describe a CME structure is a cone model. This model predicts the radial speed is greater than the observed apparent speed. Another aspect of the model is a prediction for the apparent width of the CME to increase as the CME source location moves toward disk center. This can be seen by considering a limb event with a defined angular width. If this event were observed in the top view, it would appear to be a halo, thus having an apparent angular span of 360°. In this section we also describe how basic CME properties are influenced by projection effects.
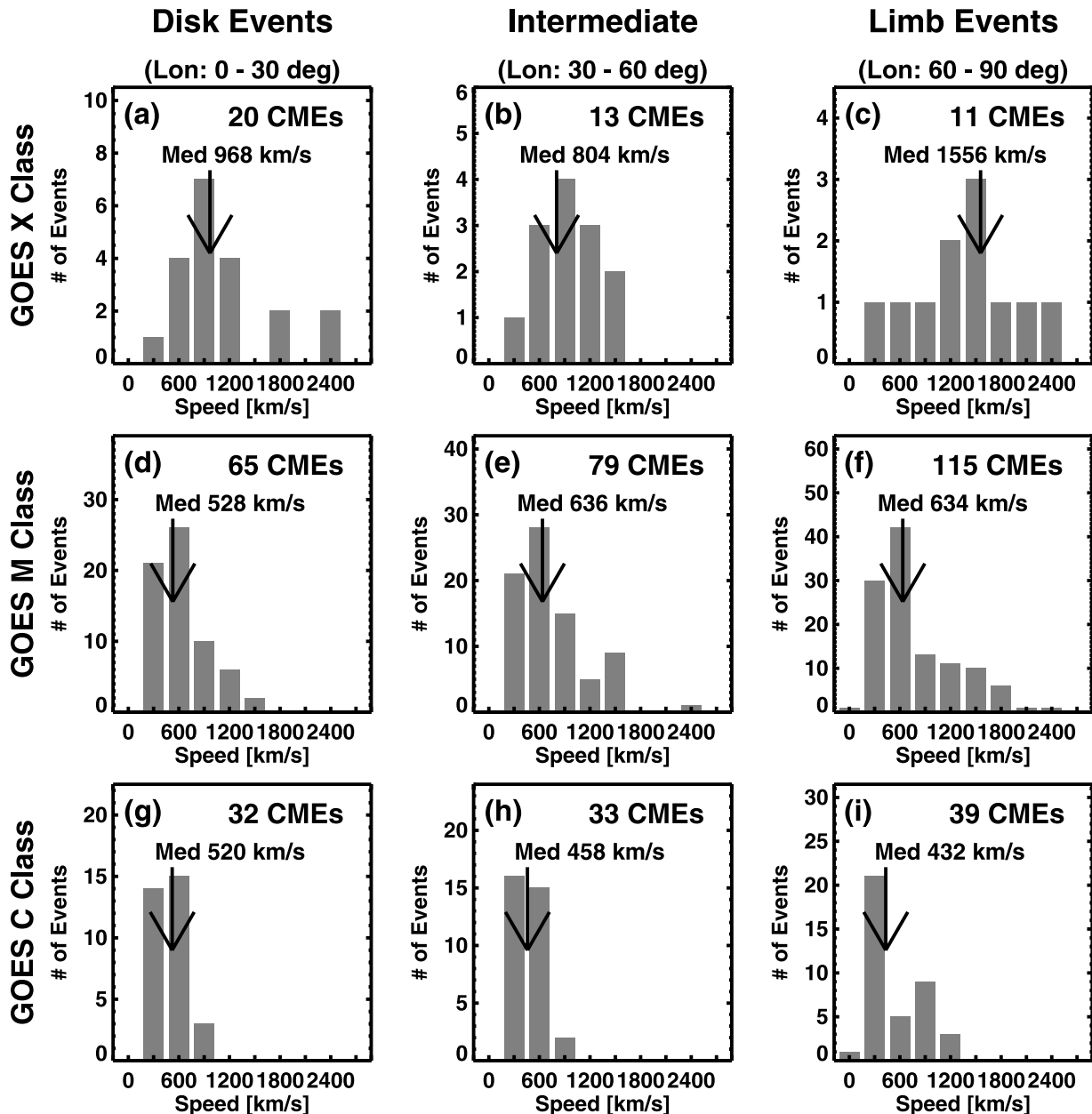
4.1. Speed Distributions

[22] Figure 3 shows the apparent speed distribution of the CMEs associated with X-, M-, and C-class flares (top, middle, and bottom, respectively) for disk, intermediate, and limb events (left, center, and right, respectively). The arrows in each plot indicate the median speed of the distributions. The median speeds of the CMEs associated with limb X-class flares (1556 km/s) were three times more than those with limb C-class flares (432 km/s). Clearly, the CME speeds increased with the size of associated flares for all longitudes.

[23] For C-class flares, the three speed distributions (for disk, intermediate, and limb events; Figures 3g–3i) are very similar. The only difference is in median speeds (520 km/s, 458 km/s, and 432 km/s for disk, intermediate, and limb events, respectively). This result is in conflict with the prospect of projection effects. As we describe in section 3.1, half of the CMEs associated with C-class flares were invisible; thus the disk events are biased. It is not unreasonable to think that slow, narrow, and faint CMEs were excluded from the disk events. Therefore the result, that limb CMEs associated with C-class flares were slower than disk CMEs, is probably from the sampling effects of the visibility of LASCO coronagraphs. On the other hand, since there was no visibility effect for the CMEs with X-class flares and a small visibility effect for the CMEs with M-class flares, the difference between limb and disk events probably indicates the difference between side and top views of CMEs. The median speeds of CMEs associated with X-class flares are 968 km/s and 1556 km/s for disk and limb events, respectively. Clearly, the disk CMEs appeared to be slower than limb CMEs. For M-class flares, the speed distributions are in between those for X- and C-class flares. The three speed distributions for disk, intermediate, and limb events (Figures 3d–3f) are very similar, but their median speed increases from limb to disk as expected from the projection effects. The median speeds of the CMEs associated with M-class flares are 528 km/s, 636 km/s, and 634 km/s for disk, intermediate, and limb events, respectively. Therefore the median speed of limb CMEs was 20–50% faster than that of disk CMEs. *Michalek et al.* [2003] investigated asymmetric halo CMEs by a cone model and estimated that the real ejection speed is 20% faster than the observed speed. This is similar to our value.
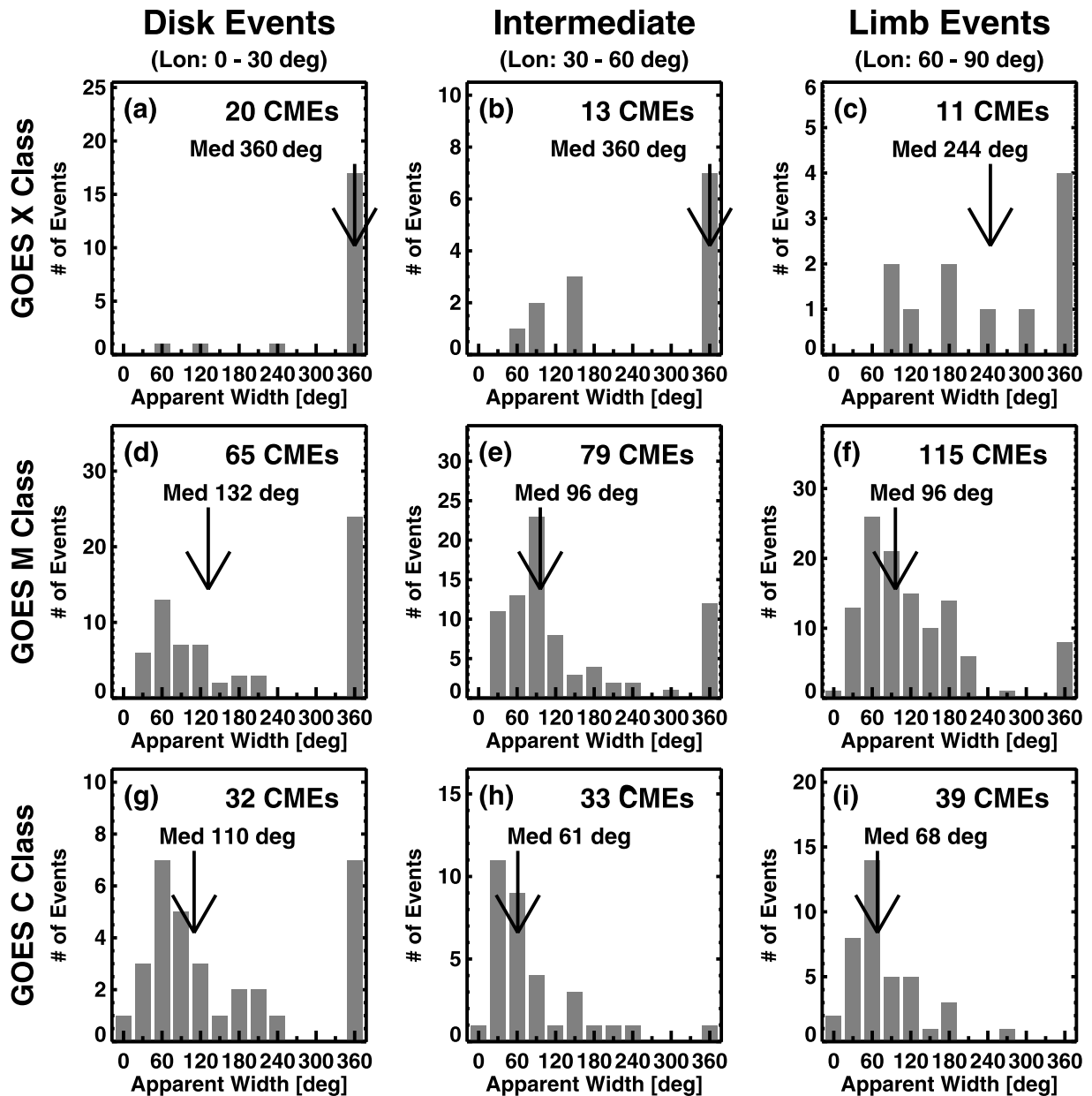
4.2. Angular Width Distributions

[24] Figure 4 shows the apparent angular width distribution of CMEs associated with X-, M-, and C-class flares

Figure 3. Distribution of apparent CME speed by latitude of flare location (left to right) and flare class (top to bottom).

(top, middle, and bottom, respectively) for disk, intermediate, and limb events (left, center, and right, respectively). The arrows in each plot indicate the median width of the distributions. For all three flare classes, the median of apparent angular width increased from limb to disk, as we expect from the point of view of the projection effects. The limb events are better for investigating the inherent CME angular widths, but in all three longitudes, the apparent angular width clearly increased with the size of associated flares. Thus the CMEs associated with large flares are likely to be inherently wide. This result is similar to *Kahler et al.* [1989], who found a correlation between the apparent angular width of CMEs and duration of flares, since large flares are likely to be long-lived.

[25] For the disk X-class flares, 17 out of 20 (85%) CMEs were observed as halos. Even for limb events, four out of 11 (36%) CMEs associated with X-class flares were halos. We should note that all limb halo CMEs appeared asymmetric. The bright CME core appeared above the flare site and a faint wave-like structure propagated above the opposite limb [*Sheeley et al.*, 2000; *Gopalswamy et al.*, 2003; *St. Cyr*, 2005]. On the other hand, even for disk events, the fractions of halo CMEs were 37% (24/65) for M-class and 22% (7/32) for C-class events. Only 7% (8/115) of CMEs associated with limb M-class flares were halos, and no halo CME associated with limb C-class flares was observed. These fractions are much smaller than those of the CMEs associated with X-class flares. Therefore inherent CME

Figure 4. Distribution of apparent CME width by longitude of flare location (left to right) and flare class (top to bottom).

angular width is obviously an important factor in deciding whether a CME would be observed as a halo.

[26] The projection effects on angular width can be seen clearly in the fraction of halo CMEs. However, if we ignore the halo CMEs, all the distributions look similar. In order to check their difference without halo CMEs, box plots of angular distributions are shown in Figure 5. The box plot summarizes a distribution by five representative points. The first and last lines indicate the minimum and maximum of the distribution, and the three lines that form the box indicate 25%, 50%, and 75% of data, respectively (see Figure 5a). Therefore the box's main body includes half of the distribution. The box plot for the CMEs associated with disk X-class flares could not be made, since we have only three nonhalo CMEs. In Figure 5b, we still can see the increasing of angular width from C-class to X-class flares

even if we exclude the halo CMEs. However, the increasing width from limb to disk events due to projection effects cannot be seen anymore.

4.3. Final Measurement Height Distributions

[27] The heights of the leading edges (LEs) of CMEs are measured as long as the feature on the LEs used for measurements can be tracked within the LASCO/C3 FOV ($\sim$32 R_S). Since a brighter CME can be tracked farther from the Sun, the final point of the height measurement can be used as a proxy of CME brightness. We should note here that this parameter depends on the observational cadence of LASCO C3. If we do not have C3 observations, we can only obtain the lower limit. *St. Cyr et al.* [2000] and *Gopalswamy* [2004] examined the final height distribution for all LASCO CMEs. The study periods were different, but
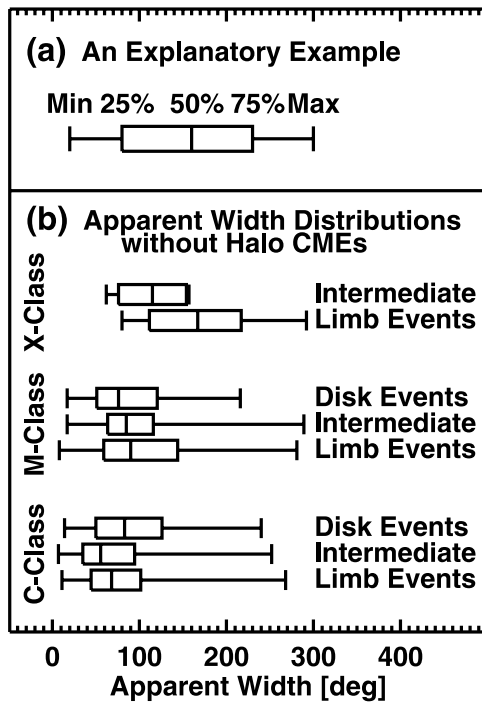
Figure 5. (a) An example of a box plot. The first and last lines indicate minimum and maximum of the distribution and three lines that form the box indicate 25%, 50%, and 75% of data, respectively. (b) Distribution of apparent width of nonhalo CMEs by longitude of flare location (marked at right) and flare class (marked at left).

the obtained distributions were quite similar. They found that about only half of the CMEs were tracked beyond 12–14 R_S.

[28] Figure 6 shows the final measurement height distribution of CMEs associated with X-, M-, and C-class flares (top, middle, and bottom, respectively) for disk, intermediate, and limb events (left, center, and right, respectively). The arrows in each plot indicate the median final measurement height. The CMEs, whose leading edge did not fade within the LASCO/C3 FOV, were included in the last bin. The peaks of the three distributions for X-class are the last bin (30+); thus approximately half (45% or 20/44) of the CMEs associated with X-class flares are found to cross the LASCO/C3 FOV.

[29] The projection effects of the final measurement heights are similar to those of the CME speed because both parameters are determined from the CME height projected onto the sky plane. The projection effects can be seen in the distributions for X- and M-class flares. Limb CMEs can be tracked to a farther height than disk CMEs. Since about half of the disk CMEs are invisible for C-class flares, there is a sampling effect also. It is not unreasonable to think that slow, narrow, and faint CMEs were excluded from the disk events, and this can be seen in the lack of CMEs disappearing quickly (see 5 R_S bin of Figure 6g). Therefore projection effects are mixed with sampling effects.

[30] Limb events are the best for investigating the relation between final measurement heights and associated flare size. The median value increased more than twice from 12 R_S (C-class) to 29 R_S (X-class). The percentage of

CMEs, which could be tracked up to the edge of the LASCO FOV, was 55% (6/11) for X-class, 22% (25/115) for M-class, and 10% (4/39) for C-class flares, respectively. The final measurement height clearly increased with associated flare sizes. These results suggest that the CMEs associated with X-class flares are likely to be brighter than those with C-class flares.

5. Summary and Discussions

[31] We investigated the association of CMEs with 1301 X-ray flares occurring from 1996 to 2001 and found that (1) the CME association rate increased from 20% for C-class flares (between C3 and C9 levels) to 100% for large flares (above X3 level), and (2) four out of the 49 X-class flares were not associated with CMEs. The lack of a CME for these prominent flares might have important implications for understanding the flare-CME relationship. With the assumption of all limb CMEs being detectable by LASCO, we determined visibility functions from the longitudinal variation of the CME association with X-ray flares. We found that (3) all disk CMEs associated with X-class flares were detectable, (4) about 84% of disk CMEs associated with M-class flares were detectable, (5) half of the disk CMEs associated with C-class flares are not visible to LASCO coronagraphs. We also examined the basic properties (speed, angular width, and final measurement height) of flare-associated CMEs and compared them not only for the different flare classes but also for the flare locations. We found that (6) the CMEs associated with X-class flares were more likely to be prominent (fast, wide, and bright) than the CMEs with C-class flares, and (7) the projection effects of the three basic properties are only seen in the medians for the CMEs with X- and M-class flares. For C-class flares, projection effects are mixed with sampling effects due to the invisible CMEs.

[32] The prominent (weak) CMEs are likely to be associated with X-class (C-class) flares. This is consistent with the fact that the fraction of invisible CMEs decreases with the size of associated flares. Because of projection effects, narrow CMEs originating from disk center need to reach a larger heliocentric distance to enter the LASCO C2 FOV. Some of the narrow CMEs fade out below the occulting disk, since the brightness decreases with the heliocentric distance. It is reasonable to think that only weak CMEs are invisible to LASCO when they originate from close to the disk center. This idea is consistent with the fact that not all CMEs associated with M-class flares were wider and brighter than CMEs associated with C-class flares. Of the 115 limb CMEs associated with M-class flares, 22 (19%) were narrower and fainter than the median CMEs associated with C-class flares. This percentage is similar to the fraction of invisible CMEs associated with M-class flares. Thus these weak CMEs could become invisible CMEs. Therefore LASCO coronagraphs observe all prominent CMEs, which are likely to be associated with large flares. However, some weak CMEs associated with average or small flares originating from close to the disk center may be invisible.

[33] Here we should note that the invisible CMEs are classified into two groups. One is undetectable CMEs, whose signal is the same or less than the background noise level. The other is unidentified CMEs, whose signal is
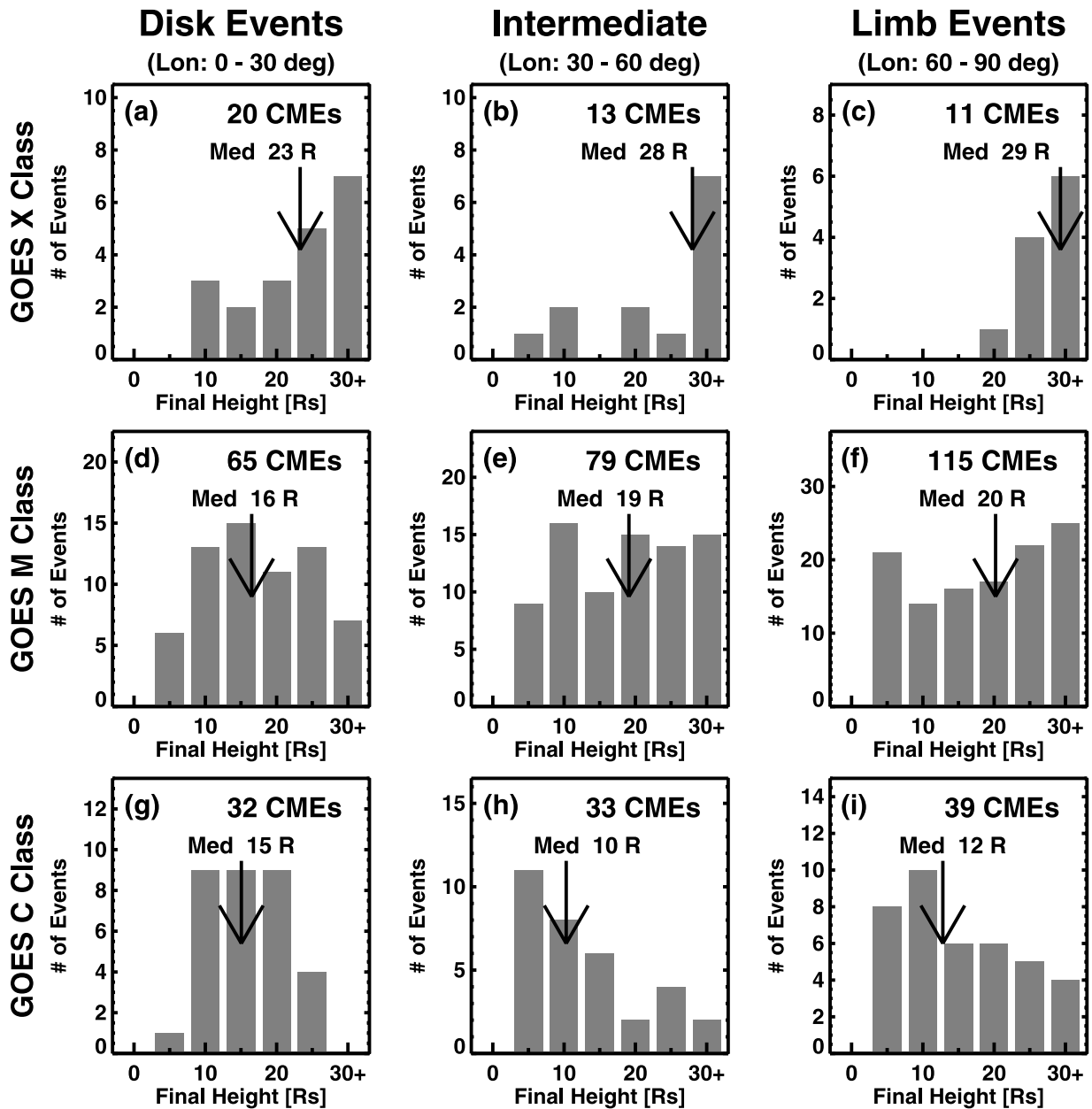
Figure 6. Distribution of final measurement heights by longitude of flare location (left to right) and flare class (top to bottom). Since the brighter CMEs are visible to farther distance (height) from the Sun, the final measurement heights of the CMEs can be used as a proxy of their brightness.

above the noise level but cannot be recognized as a CME. This happens if a CME fades out quickly and only a single image is available with sufficient CME signal. Since we have identified CMEs as moving features, a single image is not sufficient to identify the faint narrow CMEs. (For the bright wide CMEs, single image is sufficient since we can identify them from their structure.) We emphasize that this misidentification is not from careless examination but from the limitations of manual CME identification. An automated CME identification [e.g., *Robbrecht and Berghmans*, 2004] or an image emphasizing technique [e.g., *Stenborg and Cobelli*, 2003] may help to identify more faint CMEs originating from disk center.

[34] Table 3 summarizes the visibility function of LASCO CMEs associated with X-, M-, and C-class flares. We assumed that all limb CMEs are detectable by the LASCO coronagraphs, thus visibility of all limb events (fourth column) is 100%. The visibility function of CMEs with flare longitude in the range 30°–59° (intermediate events) was determined from the ratio of CME associations between limb and intermediate events. The visibility functions for all longitudes were calculated from the average of disk, intermediate, and limb events. There were 814 M-class and 2956 C-class (above C3 level) flares from 1996 through 2001. If we assume that the inherent CME association rates of flares were obtained from limb events, there were 415

Table 3. Visibility of LASCO CMEs Associated With X-Ray Flares

Class	Disk Events	Intermediate	Limb Events[a]	All
X	100%	100%	100%	100%
M	84%	100%	100%	95%
	(63–100%)	(77–100%)		(80–100%)
C	50%	67%	100%	72%
	(33–75%)	(44–100%)		(59–92%)

[a]The visibility of limb CMEs was assumed to be 100%.

(51% of 814) and 887 (30% of 2956) CMEs associated with M-class and C-class flares, respectively. From the visibility functions, we found that 21 (5% of 415) and 248 (28% of 814) frontside CMEs associated with M-class and C-class flares, respectively, were not able to be detected by LASCO. Note that this is a possible underestimate since we do not count invisible CMEs associated with small flares (below C3 level).

[35] We estimate that more than 269 frontside CMEs could be missed from 1996 through 2001, even though LASCO operated normally. In the same period, 5301 CMEs were observed by LASCO. Since LASCO detects backside events as being the same as frontside events, we can roughly say that approximately half of the 5301 CMEs were frontside events. Therefore the fraction of invisible CMEs is more than 10%, which is not negligible in counting the total number of CMEs. However, the geoeffectiveness of these invisible CMEs by themselves may not be high. Since the invisible CMEs seem to have smaller angular width, the probability of their Earth impact is lower than that of wide CMEs. Since the main drivers of large geomagnetic storms are halo CMEs [*Webb et al.*, 2000; *Zhang et al.*, 2003; *Gopalswamy*, 2004], which is an energetic population, invisible CMEs may not produce geomagnetic storms by themselves; however, the invisible CMEs may contribute to complex geomagnetic storms with intense CMEs or high-speed solar wind from coronal holes.

References

Andrews, M. D. (2002), The front-back asymmetry of coronal emission, *Sol. Phys.*, 208, 317.

Andrews, M. D. (2003), A search for CMEs associated with big flares, *Sol. Phys.*, 218, 261.

Biesecker, D. A., D. C. Myers, B. J. Thompson, D. M. Hammer, and A. Vourlidas (2002), Solar phenomena associated with "EIT waves," *Astrophys. J.*, 569, 1009.

Brueckner, G. E., et al. (1995), The Large Angle Spectroscopic Coronagraph (LASCO), *Sol. Phys.*, 162, 357.

Burkepile, J. T., A. J. Hundhausen, and J. A. Seiden (1994), A study of GOES X-ray events associated with coronal mass ejections: 1986, in *Proceedings of the Third SOHO Workshop*, ESA SP-373, p. 57, Eur. Space Agency, Paris.

Burkepile, J. T., A. J. Hundhausen, A. L. Stanger, O. C. St. Cyr, and J. A. Seiden (2004), Role of projection effects on solar coronal mass ejection properties: 1. A study of CMEs associated with limb activity, *J. Geophys. Res.*, 109, A03103, doi:10.1029/2003JA010149.

Cliver, E. W., M. Laurenza, M. Storini, and B. J. Thompson (2005), On the origins of solar EIT waves, *Astrophys. J.*, in press.

Domingo, V., B. Fleck, and A. I. Poland (1995), The SOHO mission: An overview, *Sol. Phys.*, 162, 1.

Feynman, J., and A. J. Hundhausen (1994), Coronal mass ejections and major solar eruptive events: The great active center of March 1999, *J. Geophys. Res.*, 99, 8451.

Gopalswamy, N. (2004), A global picture of CMEs in the inner heliosphere, in *The Sun and Heliosphere as an Integrated System*, edited by G. Poletto and S. T. Suess, p. 201, Springer, New York.

Gopalswamy, N., M. L. Kaiser, B. J. Thompson, L. F. Burlaga, A. Szabo, A. Lara, A. Vourlidas, S. Yashiro, and J.-L. Bougeret (2000), Radio-rich solar eruptive events, *Geophys. Res. Lett.*, 27, 1427.

Gopalswamy, N., A. Lara, M. L. Kaiser, and J.-L. Bougeret (2001), Near-Sun and near-Earth manifestations of solar eruptions, *J. Geophys. Res.*, 106, 26,261.

Gopalswamy, N., A. Lara, S. Yashiro, S. Nunes, and R. A. Howard (2003), Coronal mass ejection activity during solar cycle 23, in *Solar Variability as an Input to the Earth's Environment*, ESA SP-535, edited by A. Wilson, pp. 403–414, Eur. Space Agency, Paris.

Gosling, J. T., E. Hildner, R. M. MacQueen, R. H. Munro, A. I. Poland, and C. L. Ross (1976), The speeds of coronal mass ejection events, *Sol. Phys.*, 48, 389.

Green, L. M., S. A. Matthews, L. van Driel-Gesztelyi, L. K. Harra, and J. L. Culhane (2002), Multi-wavelength observations of an X-Class flare without a coronal mass ejection, *Sol. Phys.*, 205, 325.

Harrison, R. A. (1986), Solar coronal mass ejections and flares, *Astron. Astrophys.*, 162, 283.

Howard, R. A., D. J. Michels, N. R. Sheeley Jr., and M. J. Koomen (1982), The observation of a coronal transient directed at Earth, *Astrophys. J.*, 263, L101.

Howard, R. A., et al. (1997), Observations of CMEs from SOHO/LASCO, in *Physics of the Magnetopause*, Geophys. Monogr. Ser., vol. 99, edited by P. Song, B. U. Ö. Sonnerup, and M. F. Thomsen, pp. 17–26, AGU, Washington, D. C.

Hundhausen, A. J. (1993), Sizes and locations of coronal mass ejections: SMM observations from 1980 and 1984–1989, *J. Geophys. Res.*, 98, 13,177.

Hundhausen, A. J., J. T. Burkepile, and O. C. St. Cyr (1994), Speeds of coronal mass ejections: SMM observations from 1980 and 1984–1989, *J. Geophys. Res.*, 99, 6543.

Kahler, S. W. (1992), Solar flares and coronal mass ejections, *Annu. Rev. Astron. Astrophys.*, 30, 113.

Kahler, S. W., N. R. Sheeley Jr., R. A. Howard, M. J. Koomen, and D. J. Michels (1984), Characteristics of flares producing metric type II bursts and coronal mass ejections, *Sol. Phys.*, 93, 133.

Kahler, S. W., N. R. Sheeley Jr., and M. Liggett (1989), Coronal mass ejections and associated X-ray flare durations, *Astrophys. J.*, 344, 1026.

Leblanc, Y., G. A. Dulk, A. Vourlidas, and J.-L. Bougeret (2001), Tracing shock waves from the corona to 1 AU: Type II radio emission and relationship with CMEs, *J. Geophys. Res.*, 106, 25,301.

MacQueen, R. M., and R. R. Fisher (1983), The kinematics of solar inner coronal transients, *Sol. Phys.*, 89, 89.

Michalek, G., N. Gopalswamy, and S. Yashiro (2003), A new method for estimating widths, velocities, and source location of halo coronal mass ejections, *Astrophys. J.*, 584, 472.

Moon, Y. J., G. S. Choe, H. Wang, Y. D. Park, N. Gopalswamy, G. Yang, and S. Yashiro (2002), A statistical study of two classes of coronal mass ejections, *Astrophys. J.*, 581, 694.

Munro, R. H., J. T. Gosling, E. Hildner, R. M. MacQueen, A. I. Poland, and C. L. Ross (1979), The associations of coronal mass ejection transients with other forms of solar activity, *Sol. Phys.*, 61, 201.

Robbrecht, E., and D. Berghmans (2004), Automated recognition of coronal mass ejections (CMEs) in near-real-time data, *Astron. Astrophys.*, 425, 1097.

Sawyer, C. (1985), Visibility and rate of coronal mass ejections, *Sol. Phys.*, 98, 369.

Sheeley, N. R., et al. (2000), Detection of coronal mass ejection associated shock waves in the outer corona, *J. Geophys. Res.*, 105, 5081.

St. Cyr, O. C. (2005), The last word: The definition of halo coronal mass ejections, *Eos Trans. AGU*, 86(30), 281.

St. Cyr, O. C., et al. (2000), Properties of coronal mass ejections: SOHO LASCO observations from January 1996 to June 1998, *J. Geophys. Res.*, 105, 18,169.

Stenborg, G., and P. J. Cobelli (2003), A wavelet packets equalization technique to reveal the multiple spatial-scale nature of coronal structures, *Astron. Astrophys.*, 398, 1185.

Vourlidas, A., P. Subramanian, K. P. Dere, and R. A. Howard (2000), Large angle spectrometric coronagraph measurements of the energetics of coronal mass ejections, *Astrophys. J.*, *534*, 456.

Webb, D. F., and R. A. Howard (1994), The solar cycle variation of coronal mass ejections and the solar wind mass flux, *J. Geophys. Res.*, *99*, 4201.

Webb, D. F., E. W. Cliver, N. U. Crooker, O. C. St. Cyr, and B. J. Thompson (2000), Relationship of halo coronal mass ejections, magnetic clouds, and magnetic storms, *J. Geophys. Res.*, *105*, 7491.

Yashiro, S., N. Gopalswamy, G. Michaek, O. C. St. Cyr, S. P. Plunkett, N. B. Rich, and R. A. Howard (2004), A catalog of white light coronal mass ejections observed by the SOHO spacecraft, *J. Geophys. Res.*, *109*, A07105, doi:10.1029/2003JA010282.

Zhang, J., K. P. Dere, R. A. Howard, and V. Bothmer (2003), Identification of solar sources of major geomagnetic storms between 1996 and 2000, *Astrophys. J.*, *582*, 520.

───────────────

S. Akiyama, N. Gopalswamy, and S. Yashiro, NASA Goddard Space Flight Center, Code 695.0, Greenbelt, MD 20771, USA. (yashiro@cdaw.gsfc.nasa.gov)

R. A. Howard, Solar Physics Branch, Space Science Division, Naval Research Laboratory, Washington, DC 20375, USA. (russ.howard@nrl.navy.mil)

G. Michalek, Astronomical Observatory of Jagiellonian University, ul. Orla 171, Krakow 30-244, Poland. (michalek@oa.uj.edu.pl)